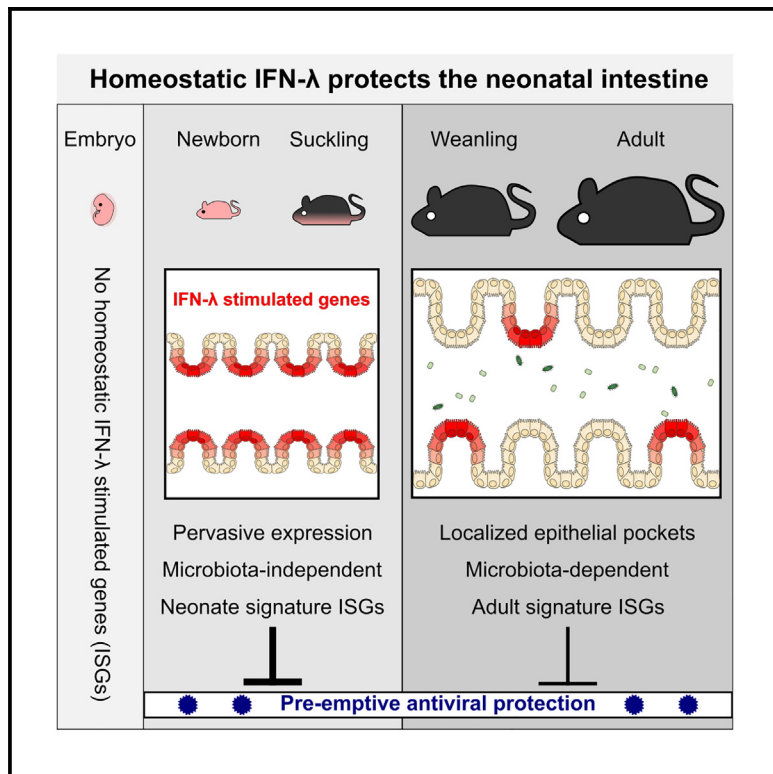


Homeostatic antiviral protection of the neonatal gut epithelium by interferon lambda

Graphical abstract



Authors

Bryan Ramirez Reyes, Shelby Madden,
Kimberly A. Meyer, Brenden Bartsch,
Austin P. Wright, David A. Constant,
Timothy J. Nice

Correspondence

nicet@ohsu.edu

In brief

Enteric viral infections are a major public health problem in newborns. Ramirez Reyes et al. find that the immature intestinal epithelium of newborn mice is developmentally programmed for the homeostatic expression of antiviral genes. These homeostatic responses depend on type III interferon and provide preemptive protection from enteric viral infection.

Highlights

- Antiviral genes are widespread in the neonatal intestine epithelium at homeostasis
- Homeostatic antiviral genes limit rotavirus infection of neonatal epithelial cells
- Homeostatic antiviral genes in the neonatal intestine require IFN-λ
- IFN-λ-stimulated genes of the neonatal intestine are developmentally programmed



Article

Homeostatic antiviral protection of the neonatal gut epithelium by interferon lambda

Bryan Ramirez Reyes,¹ Shelby Madden,¹ Kimberly A. Meyer,¹ Brenden Bartsch,¹ Austin P. Wright,¹ David A. Constant,¹ and Timothy J. Nice^{1,2,*}

¹Department of Molecular Microbiology and Immunology, Oregon Health and Science University, Portland, OR 97239, USA

²Lead contact

*Correspondence: nice@ohsu.edu

<https://doi.org/10.1016/j.celrep.2025.115243>

SUMMARY

Cell-intrinsic antiviral gene expression by intestinal epithelial cells (IECs) limits infection by enteric viral pathogens. Here, we find that neonatal IECs express antiviral genes at homeostasis that depend on interferon lambda (IFN-λ) and are required for early control of mouse rotavirus (mRV) infection. Neonatal homeostatic IFN-λ responses are independent of microbiota and pervasively distributed among IECs, distinguishing them from the homeostatic responses of adult mice. Developmental differences in homeostatic IFN-stimulated gene signatures of the intestine are regulated by maturation during the suckling-to-weanling transition, which includes reduced expression of Prdm1 by mature IECs. These studies identify developmental regulation of the homeostatic IFN-λ response, which is present in the neonatal intestine from birth, stimulated independent of microbiota, and preemptively protects IECs from viral infection. This intrinsically programmed antiviral response in early life is particularly important due to the absence of a robust microbiota or protective immune memory at birth, when the risk of enteric infection is high.

INTRODUCTION

The gastrointestinal epithelium must be tolerant of beneficial microbiota but also represents the first cellular barrier to infection by enteric pathogens. Human rotaviruses are a major contributor to the global burden of gastrointestinal infection¹ and selectively infect intestinal epithelial cells (IECs) within the small intestine (SI) to trigger diarrheal disease. Rotaviruses are highly species specific, and murine rotavirus (mRV) strains have been identified as agents that cause diarrheal disease in neonatal mice and used to develop a small animal model of rotavirus disease.^{2,3} All mice are susceptible to mRV infection, but only young mice develop diarrheal disease.⁴ This age dependency is reflective of human rotavirus disease and emphasizes the importance of understanding how the intestinal immune response to infections differs with age.

Interferons (IFNs) are a family of cytokines with important roles in controlling viral infection. Signaling through IFN receptors initiates the transcription of IFN-stimulated genes (ISGs), which collectively establish an antiviral state within the responding cell.⁵ There are three different types of IFNs, classified based on their use of distinct cell surface receptors.⁶ Type III IFN (hereafter, IFN lambda [IFN-λ]) is important for the antiviral protection of epithelial cells in diverse tissues due to preferential expression of the IFN-λ receptor *Ifnlr1* on epithelial lineages.^{7,8} IFN-λ is necessary for the control of enteric viral infections that target IECs, with minimal contributions of type I or II IFN.^{9–12} The partic-

ular importance of IFN-λ in the gut may be due to the relatively low expression of the type I IFN receptor IFNAR (IFN alpha receptor) on mature IECs^{12,13} and suggests that protective roles in the intestinal epithelium are highly relevant to the evolution and biology of IFN-λ.

In the gut, homeostatic immune responses can be crucial for fostering a peaceful co-existence with beneficial microbiota and can also act as a preemptive barrier to infection by pathogens. We previously reported the presence of homeostatic IFN-λ responses in the gastrointestinal epithelium of adult mice.¹⁴ These homeostatic IFN-λ responses were present in localized pockets of the intestinal epithelium and stimulated by the presence of bacterial microbiota. Homeostatic IFN-λ responses provided preemptive protection against mRV infection of adult IECs within the first day of infection.¹⁴ Due to the age dependency of rotavirus disease and microbiota acquisition, the present study aimed to define the developmental time course of the intestinal homeostatic IFN-λ response and its role in the protection of the neonatal epithelium. We found that a homeostatic IFN-λ response was present in mouse IECs from birth and protected against rotavirus infection and disease. In contrast to adult mice, homeostatic ISG expression in neonatal mouse intestines was independent of the microbiota and widely distributed across the epithelium. These data indicate that a protective homeostatic IFN-λ response is present from birth and mechanistically distinct from the corresponding response in adults. We propose that the neonatal homeostatic



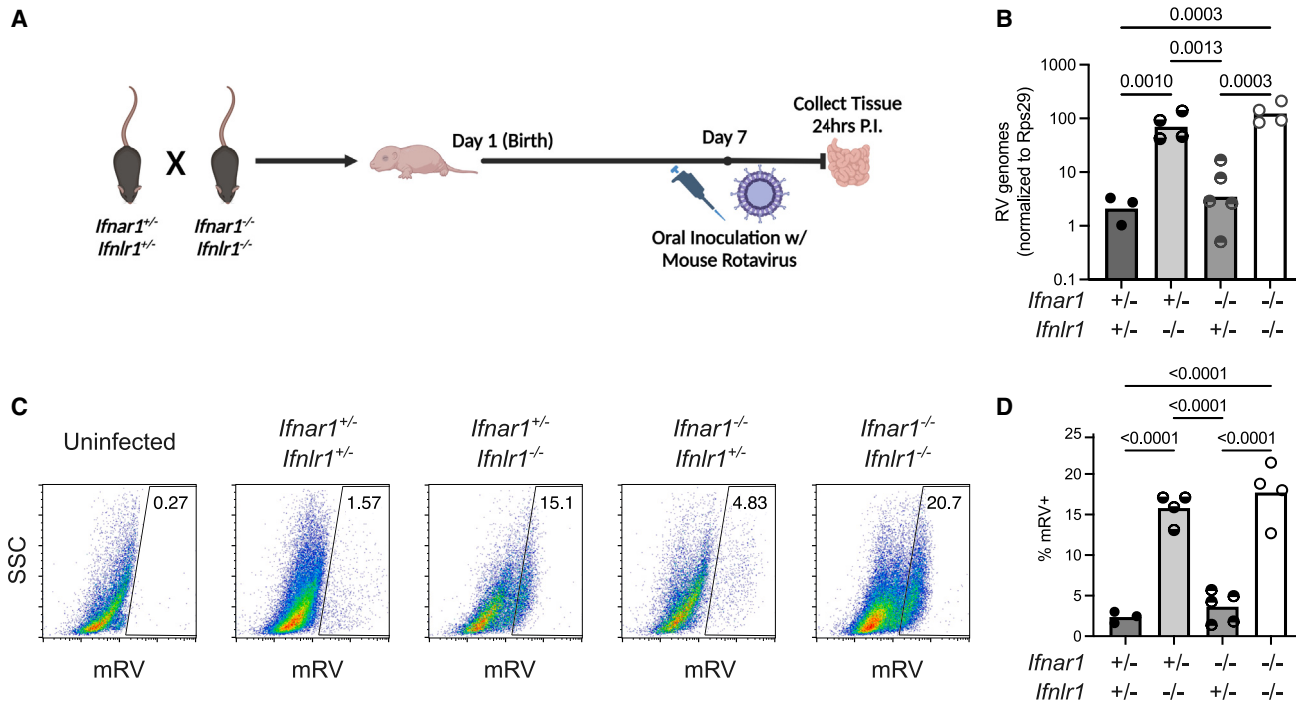


Figure 1. Interferon lambda limits IEC infection during the first day of rotavirus exposure

(A) Diagram of the experimental setup. Seven-day-old littermates from *Ifnlr1*^{+/−} *Ifnar1*^{+/−} × *Ifnlr1*^{−/−} *Ifnar1*^{−/−} mating pairs were orally inoculated with mRV. IECs were isolated from intestinal tissue 24 h post-inoculation (P.I.) for quantification of viral replication.

(B) mRV genomes were quantified via qPCR.

(C) and (D) mRV antigen was detected by flow cytometry via intracellular staining with polyclonal antisera.

(C) Representative flow plots of uninfected and mRV-infected mice of the indicated genotypes.

(D) Flow cytometry quantification of infected IECs (% mRV+) from all mice.

Statistical significance was determined by one-way ANOVA with the Tukey multiple comparison test (B and D). Each data point represents an individual mouse, and data are cumulative from two litters of mice.

IFN-λ response is intrinsically programmed to provide broad protection of the intestinal epithelium during early life, when susceptibility to viral infections is high.

RESULTS

IFN-λ limits IEC infection during the first day of rotavirus exposure

To quantify the early roles of IFN signaling in limiting mRV infection of neonatal IECs, we infected littermate mice deficient in either *Ifnlr1*, *Ifnar1*, or both and collected tissues 24 h post-inoculation (P.I.). These littermates had an ability to respond to both types of IFN (*Ifnlr1*^{+/−} *Ifnar1*^{+/−}), respond to IFN-λ only (*Ifnlr1*^{+/−} *Ifnar1*^{−/−}), respond to type I IFN only (*Ifnlr1*^{−/−} *Ifnar1*^{+/−}), or respond to neither type of IFN (*Ifnlr1*^{−/−} *Ifnar1*^{−/−}) (Figure 1A). Seven days after birth, littermates were infected with mRV, and IECs were collected 24 h P.I. for the quantification of viral genomes by qPCR (Figure 1B) and infected IECs by flow cytometry (Figure 1C). Deletion of *Ifnlr1* (*Ifnlr1*^{−/−} *Ifnar1*^{+/−} or *Ifnlr1*^{−/−} *Ifnar1*^{−/−}) resulted in a 10-fold increase of mRV genomes compared to mice capable of mounting an IFN-λ response (*Ifnlr1*^{+/−} *Ifnar1*^{−/−} or *Ifnlr1*^{−/−} *Ifnar1*^{+/−}) (Figure 1B). Flow cytometry data additionally revealed that significantly more IECs were infected in mice lacking *Ifnlr1* (10%–25% infected IECs)

compared to mice capable of mounting an IFN-λ response (1%–5% infected IECs) (Figures 1C and 1D). These data indicate that IFN-λ signaling is critical for limiting the number of infected IECs in the neonatal SI during the first day following mRV exposure, whereas type I IFN plays a minimal role.

IFN-λ responses by IECs control rotavirus infection and limit disease

To test whether IFN-λ responses required for early protection from mRV were IEC intrinsic, we inoculated neonatal littermates from *Vil1-cre*⁺ *Ifnlr1*^{flox/flox} × *Ifnlr1*^{flox/flox} breeding pairs with mRV and collected IECs 24 h P.I. for analysis (Figure 2A). Cre-positive neonates were deficient for *Ifnlr1* on *Vil1*-expressing IECs (hereafter *Ifnlr1*^{ΔIEC}), and cre-negative neonates were *Ifnlr1*-sufficient littermate controls (*Ifnlr1*^{flox/flox}). The epithelial fraction isolated from *Ifnlr1*^{ΔIEC} neonate intestines had greater than 10-fold more mRV genomes compared to littermate controls (Figure 2B). Likewise, there were significantly more mRV-infected IECs (7%–17%) in *Ifnlr1*^{ΔIEC} neonates compared to controls (~1% infected IECs) (Figures 2C and 2D). The median fluorescence intensities of mRV antigens within infected IECs were not significantly different between groups (Figure 2E), suggesting that IFN-λ blocked productive infection in the majority of IECs rather than causing reduced replication in IECs after infection.

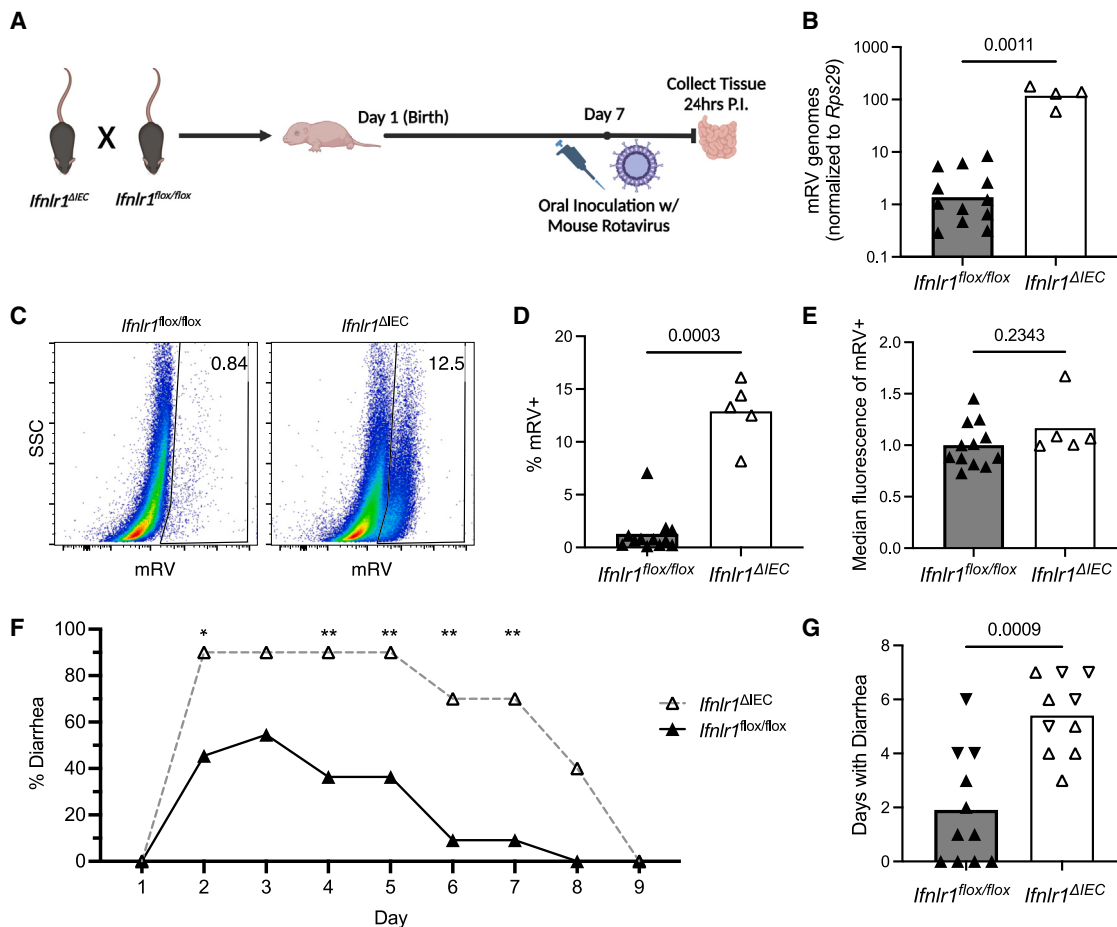


Figure 2. Interferon lambda responses by IECs control rotavirus infection and limit disease

(A) Diagram of the experimental setup. Seven-day-old littermates from *Ifnlr1^{ΔIEC}* and *Ifnlr1^{fl/fl}* mating pairs were orally inoculated with mRV. IECs were isolated from intestinal tissue 24 h post inoculation (P.I.) for quantification of viral replication.

(B) mRV genomes were quantified via qPCR.

(C–E) mRV antigen was detected by flow cytometry via intracellular staining with polyclonal antisera.

(C) Representative flow plots of uninfected and mRV-infected mice of the indicated genotypes.

(D) Flow cytometry quantification of infected IECs (% mRV⁺) from all mice.

(E) Median fluorescence intensity of mRV stain by flow cytometry.

(F and G) Four experimental replicate litters of mice were orally inoculated with mRV on post-natal day 7 and monitored daily for incidence of diarrhea.

(F) Plot showing the percentage of mice with diarrhea on each day.

(G) Plot showing the duration of diarrheal disease for *Ifnlr1^{fl/fl}* and *Ifnlr1^{ΔIEC}* neonatal mice.

Statistical significance was determined by the Mann-Whitney test (B, D, E, and G) or two-way ANOVA with the Sidak multiple comparison test (F). **p* < 0.05 and ***p* < 0.01. Each data point represents an individual mouse, and data are cumulative from three litters of mice.

Neonatal mice are susceptible to diarrheal disease caused by mRV infection. To determine whether early control of IEC infection by IFN-λ impacted the extent of subsequent disease, we quantified how many mice had diarrhea each day P.I. of four replicate groups of *Ifnlr1^{ΔIEC}* and *Ifnlr1^{fl/fl}* littermates. About 50% of *Ifnlr1^{fl/fl}* wild-type (WT) littermates exhibited diarrhea P.I. with mRV and resolved disease by day 8 P.I. (Figure 2F). In contrast, 100% of *Ifnlr1^{ΔIEC}* littermates exhibited diarrhea on at least 3 days (Figure 2G), with significantly greater incidence of diarrhea on days 2–7 P.I. (Figure 2F). The overall duration of disease was also significantly greater in *Ifnlr1^{ΔIEC}* neonates (5 days) relative to WT littermate controls (2 days) (Figure 2G). Together,

these data indicate that IEC-intrinsic IFN-λ responses limit the number of IECs infected by mRV and significantly reduce the subsequent burden of diarrheal disease.

A homeostatic IFN-λ response is present in the neonatal epithelium

The neonatal protection data above (Figures 1 and 2), together with our prior studies of adult mice,¹⁴ suggest that pre-existing homeostatic IFN-λ responses may be present in the intestines of 1-week-old neonates. To determine when homeostatic IFN-λ responses are present during post-natal development, we quantified ISG mRNAs from the proximal SI (duodenum),

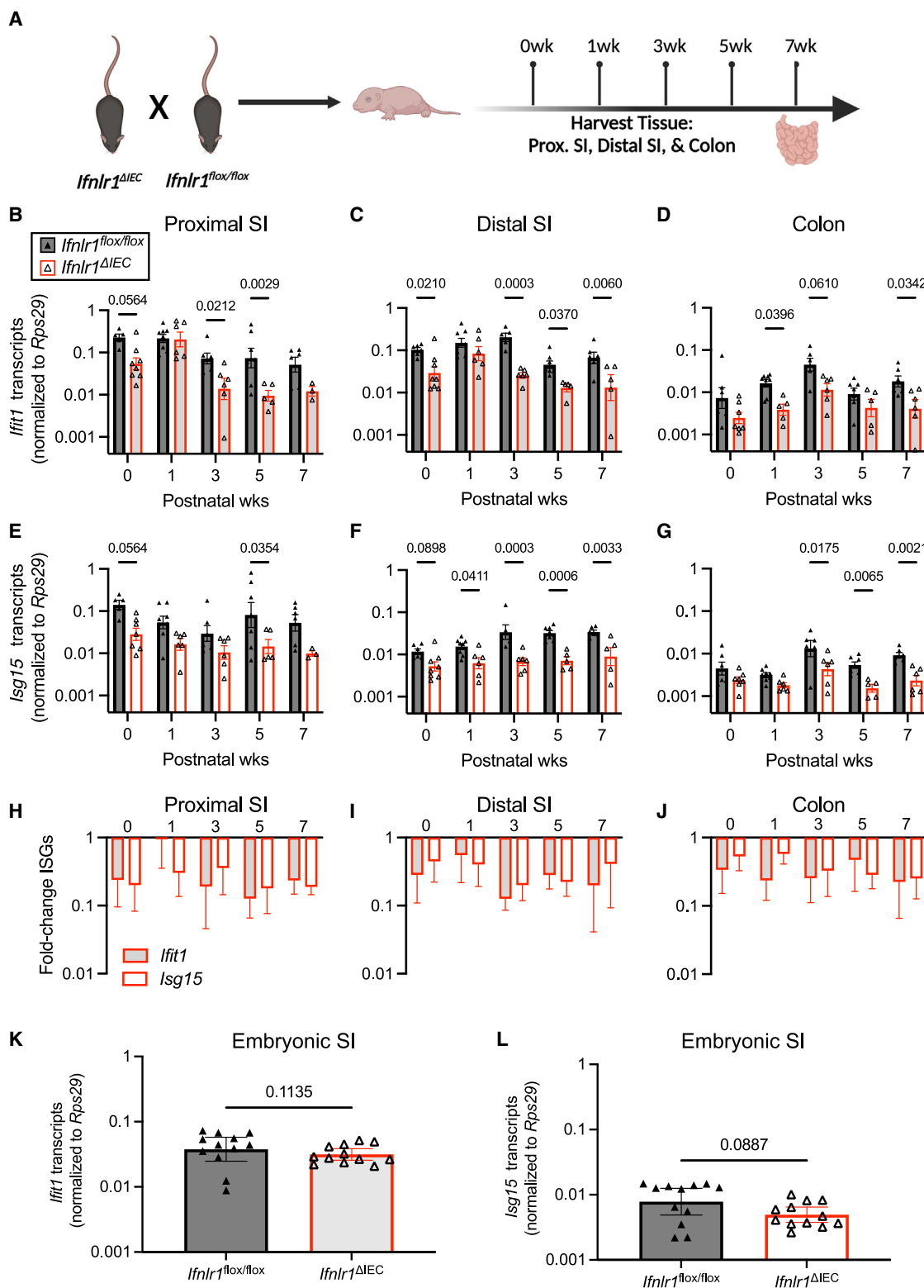


Figure 3. A homeostatic interferon lambda response is present in the neonatal epithelium

(A) Diagram of the experimental setup. Intestinal tissues were collected from *Ifnrl1* $^{\Delta IE}$ and *Ifnrl1* $^{fl/fl}$ littermates at the indicated times for quantification of ISGs in whole intestinal tissue segments by qPCR.

(legend continued on next page)

distal SI (ileum), and colon of *Ifnlr1*^{flox/flox} and *Ifnlr1*^{ΔIEC} littermates at 0 (within 2 days of birth), 1, 3, 5, and 7 weeks (Figure 3A). We selected *Iif1* and *Isg15* as representative antiviral ISGs based on their prominence within the adult homeostatic IFN-λ signature and quantified the expression in intestinal tissues by qPCR (Figures 3B–3J). ISG expression attributable to homeostatic IFN-λ signaling in IECs was determined by calculating the difference between *Ifnlr1*^{ΔIEC} and *Ifnlr1*^{flox/flox} littermate controls (Figures 3H–3J). The *Ifnlr1*^{ΔIEC} mice had a significant reduction in *Iif1* expression in the distal SI in comparison to *Ifnlr1*^{flox/flox} littermates as early as week 0 (Figure 3C). Overall, we measured a consistent decrease in ISG expression of *Ifnlr1*^{ΔIEC} mice across tissues and time points compared to *Ifnlr1*^{flox/flox} littermate controls (Figures 3H–3J). Specifically, we observed statistically significant decreases in *Iif1* transcripts from *Ifnlr1*^{ΔIEC} mice in proximal SI (0, 3, and 5 weeks), distal SI (0, 3, 5, and 7 weeks), and colon (1, 3, and 7 weeks) (Figures 3B–3D); we observed statistically significant decreases in *Isg15* transcripts from *Ifnlr1*^{ΔIEC} mice in proximal SI (0 and 5 weeks), distal SI (0, 1, 3, 5, and 7 weeks), and colon (3, 5, and 7 weeks) (Figures 3E–3G). Thus, we conclude that a homeostatic IFN-λ response is present in IECs of the gastrointestinal tract beginning in the first days after birth.

We noted that there were still substantial ISG transcripts present in intestinal tissues from *Ifnlr1*^{ΔIEC} mice (Figure 3). The residual ISG expression could represent IFN-λ responses by non-IECs, type I IFN responses within the tissue, or a combination of factors. Quantification of *Ifnlr1* expression revealed higher levels in neonatal *Ifnlr1*^{ΔIEC} small intestinal tissue compared to that of weanlings and adults (Figure S1), suggesting that there are more non-IECs expressing the IFN-λ receptor in neonates. To test the contributions of IFN types to homeostatic ISG expression at 1 week of age, we quantified ISG expression in littermates in which all cells had the ability to respond to both types of IFN (*Ifnlr1*^{+/-} *Ifnar1*^{+/-}), respond to IFN-λ only (*Ifnlr1*^{+/-} *Ifnar1*^{-/-}), respond to type I IFN only (*Ifnlr1*^{-/-} *Ifnar1*^{+/-}), or respond to neither type of IFN (*Ifnlr1*^{-/-} *Ifnar1*^{-/-}). Tissues from the proximal SI (duodenum), distal SI (ileum), and colon were harvested at 1 week after birth for quantification of *Iif1* and *Isg15* (Figure S2). We observed a decreasing trend of *Iif1* transcripts in the colon of *Ifnlr1*-deficient mice (*Ifnlr1*^{-/-} *Ifnar1*^{+/-} and *Ifnlr1*^{-/-} *Ifnar1*^{-/-}) in comparison to *Ifnlr1*-sufficient mice (*Ifnlr1*^{+/-} *Ifnar1*^{-/-} and *Ifnlr1*^{+/-} *Ifnar1*^{+/-}), suggesting that homeostatic IFN-λ specifically contributes to homeostatic *Iif1* expression in the neonatal colon. *Isg15* transcripts were significantly lower in *Ifnlr1*-deficient mice (*Ifnlr1*^{-/-} *Ifnar1*^{+/-} or *Ifnlr1*^{-/-} *Ifnar1*^{-/-}) compared to *Ifnlr1*-sufficient mice (*Ifnlr1*^{+/-} *Ifnar1*^{-/-} or *Ifnlr1*^{+/-} *Ifnar1*^{+/-}), indicating that IFN-λ is the major contributor to homeostatic *Isg15* expression in the neonatal SI (Figures S2D and S2E). Together, these

data indicate that homeostatic ISG expression within intestines of 1-week-old neonatal mice is partly dependent on IFN-λ, with relatively minimal contributions from type I IFNs.

The preceding data (Figures 3B–3J) suggested that the homeostatic IFN-λ response may be established prior to birth. To test whether the homeostatic IFN-λ response is present *in utero*, we collected the SI of *Ifnlr1*^{flox/flox} and *Ifnlr1*^{ΔIEC} littermates on embryonic day 17.5–19.5. Quantification of *Iif1* and *Isg15* via qPCR indicated that there were no significant differences in homeostatic ISG expression between embryonic *Ifnlr1*^{flox/flox} or *Ifnlr1*^{ΔIEC} SIs (Figures 3K and 3L). Additionally, the quantity of normalized ISG expression in fetal intestine was 5- to 15-fold lower than that of newborn intestine (Figures 3B, 3C, 3E, 3F, 3K, and 3L); the *Iif1* range is 0.009–0.073 copies/*Rps29* in fetal intestine vs. 0.063–0.372 in newborns and the *Isg15* range is 0.002–0.015 copies/*Rps29* in fetal intestine vs. 0.008–0.251 in newborns. Together, these data indicate that the homeostatic IFN-λ response in the intestinal tract is established at a perinatal time point, concordant with the profound physiological changes associated with a transition from fetus to newborn.

Neonatal homeostatic ISGs are not from a maternal source

We did not observe a homeostatic IFN-λ response in embryonic mice (Figures 3K and 3L), but there may be other sources of maternally derived stimulation, such as breast milk. To determine whether homeostatic IFN-λ in 1-week-old neonatal mice is derived from a maternal source, we performed a cross-fostering experiment as outlined in Figure S3A. IFN-λ-deficient (*Ifnl2/3*^{-/-}) newborns were cross-fostered to a dam capable of producing IFN-λ (*Ifnlr1*^{flox/flox} or *Ifnlr1*^{ΔIEC}). Reciprocally, *Ifnlr1*^{flox/flox} and *Ifnlr1*^{ΔIEC} littermates were cross-fostered to an *Ifnl2/3*^{-/-} dam. Seven days after cross-fostering, the proximal SI, distal SI, and colon of neonatal mice were harvested (Figure S3A). *Iif1* and *Isg15* were quantified in tissues by qPCR, and normalized transcript levels were compared between the different neonatal groups (Figures S3B–S3G). *Iif1* transcripts were significantly lower in cross-fostered *Ifnl2/3*^{-/-} neonates compared to *Ifnlr1*^{flox/flox} neonates in the proximal SI, distal SI, and colon (Figures S3B–S3D). *Isg15* transcripts were significantly lower in *Ifnl2/3*^{-/-} neonates compared to *Ifnlr1*^{flox/flox} in the proximal and distal SI (Figures S3E and S3F). Cross-fostered *Ifnlr1*^{ΔIEC} mice were phenotypically like cross-fostered *Ifnl2/3*^{-/-} mice in that they had reduced ISG expression compared to *Ifnlr1*^{flox/flox} controls. These data indicate that *Ifnl2/3* production by the neonate is necessary for homeostatic ISG expression, whereas maternal production of *Ifnl2/3* is dispensable, and suggest that a post-natal stimulus elicits IFN-λ production within the newborn intestine.

(B–G) Quantification of *Iif1* (B–D) and *Isg15* (E–G) normalized to *Rps29* (housekeeping gene) from proximal small intestine tissue (B and E), distal small intestine tissue (C and F), and colon tissue (D and G).

(H–J) *Iif1* and *Isg15* transcripts from *Ifnlr1*^{ΔIEC} mice normalized to *Ifnlr1*^{flox/flox} mice, displaying the magnitude of change in ISG transcripts when *Ifnlr1* is knocked out specifically in IECs. Tissue sites and time points for normalized data in (H)–(J) are aligned with underlying raw data in plots above.

(K and L) Quantification of *Iif1* and *Isg15* from small intestinal tissues collected at embryonic day 17.5–19.5.

Statistical significance was determined by two-way ANOVA with the Sidak multiple comparisons test (B–G) or Mann–Whitney test (K and L). Each data point represents an individual mouse, and data are cumulative from 12 (B–J) or three (K–L) litters. Data in (H)–(J) are represented as mean ± SD.

See also Figures S1 and S2.

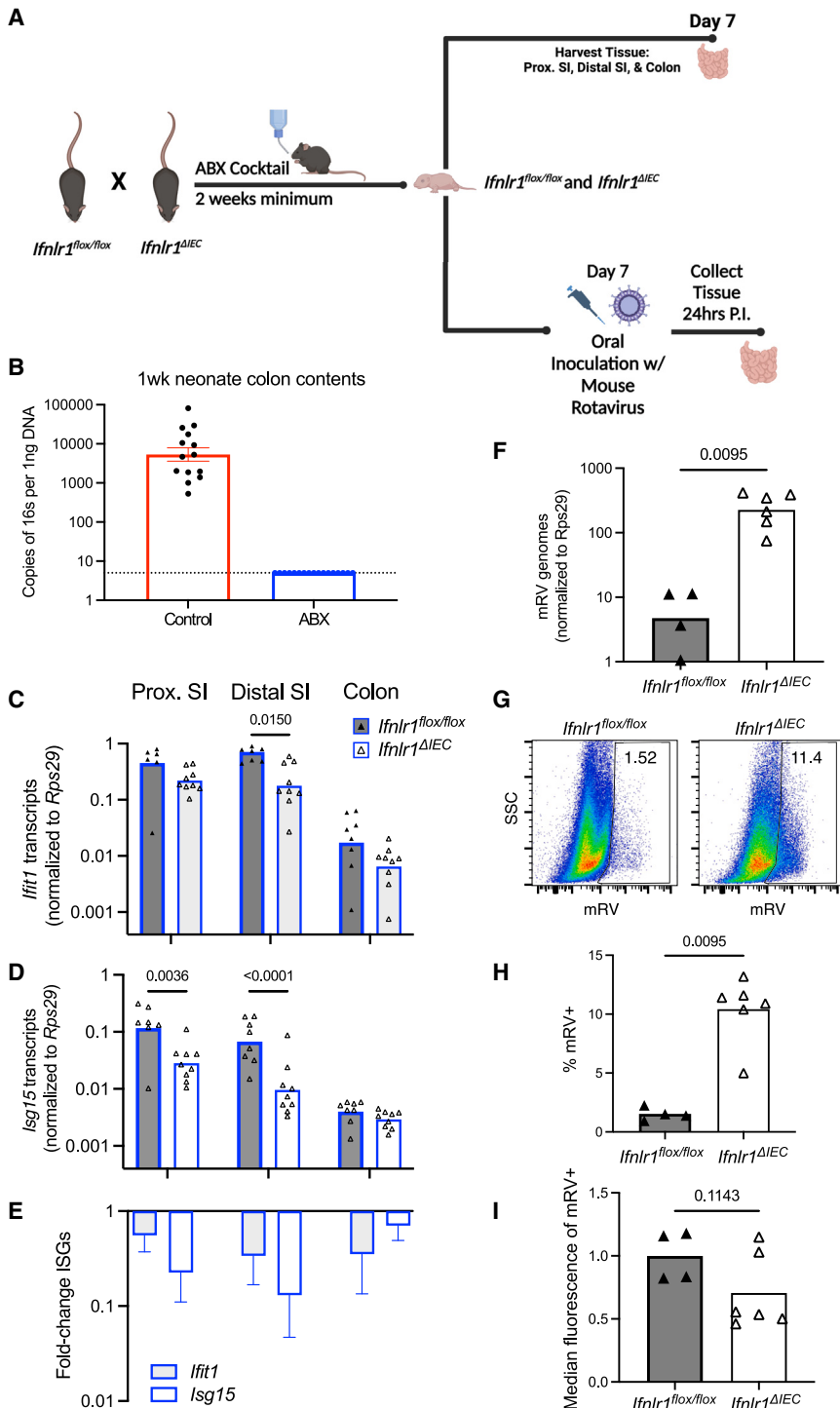


Figure 4. Neonatal homeostatic IFN lambda response is microbiota independent

(A) Diagram of experimental setup.

(B) Copies of 16S rDNA in the colon contents quantified via qPCR.

(C and D) ISG transcripts from ABX-treated *Ifnlr1*^{fl/fl} and *Ifnlr1*^{ΔIEC} mice normalized to *Rps29* from proximal small intestine, distal small intestine, and colon tissue. Statistical significance was determined by two-way ANOVA with the Sidak multiple comparison test.

(E) *Ifit1* and *Isg15* transcripts from *Ifnlr1*^{ΔIEC} mice at each respective tissue site normalized to *Ifnlr1*^{fl/fl} mice, displaying the magnitude of decrease in ISG transcripts when the *Ifnlr1* is knocked out. Tissue sites are the indicated labels above (C).

(F–I) One-week-old neonatal mice born to ABX breeders were orally inoculated with rotavirus. Intestinal tissue was collected 24 h post-inoculation. RV genomes were quantified via qPCR (F), and RV antigen was detected with intracellular antibody staining via flow cytometry (G–I). Statistical significance in (F), (H), and (I) was determined by the Mann-Whitney test. Each data point represents an individual mouse, and data are cumulative from four (B–E) or two (F–I) litters of mice. Data in (E) are represented as mean ± SD.

pairs were given an antibiotics cocktail (ABX) in the drinking water for at least 2 weeks (Figure 4A). We collected colon contents from 1-week-old neonates to verify ablation of the bacterial microbiota by 16S rDNA qPCR. Control neonates from mating pairs without the ABX had a range of 500–100,000 copies of 16S rDNA per 1 ng of colon content DNA, whereas neonates from ABX-treated mating pairs had undetectable 16S rDNA (Figure 4B). Tissue from the proximal SI, distal SI, and colon were isolated from these bacteria-depleted *Ifnlr1*^{fl/fl} and *Ifnlr1*^{ΔIEC} neonates for the quantification of ISG transcripts by qPCR (Figures 4C–4E). *Ifit1* transcripts in the distal SI were significantly decreased in *Ifnlr1*^{ΔIEC} mice compared to *Ifnlr1*^{fl/fl} mice (Figure 4C). *Isg15* transcripts in the proximal and distal SI were significantly decreased in *Ifnlr1*^{ΔIEC} mice compared to *Ifnlr1*^{fl/fl} mice (Figure 4D). Overall, ISGs were lower in ABX-treated

Ifnlr1^{ΔIEC} mice compared to ABX-treated *Ifnlr1*^{fl/fl} mice (Figure 4E), indicating the presence of a homeostatic IFN-λ response. These data indicate that the neonatal homeostatic IFN-λ response is independent of bacterial microbiota and therefore mechanistically distinct from the homeostatic IFN-λ response of adult mice.

Neonatal homeostatic IFN-λ response is microbiota independent

The stimulus for homeostatic IFN-λ responses in adult mice is colonization of the intestine by bacterial microbiota.¹⁴ To determine whether the neonatal homeostatic IFN-λ response also requires bacterial microbiota, *Ifnlr1*^{fl/fl} and *Ifnlr1*^{ΔIEC} mating

To test whether the microbiota-independent IFN- λ response is important for the protection of IECs, we infected 1-week-old ABX-treated *Ifnlr1*^{-IEC} and *Ifnlr1*^{fl/fl} neonatal mice with mRV and collected epithelial fractions from the SI 24 h later (Figures 4F–4I). ABX-treated *Ifnlr1*^{-IEC} neonates had greater than 10-fold more mRV genomes in their epithelial fraction compared to control littermates (Figure 4F). Likewise, there were significantly more mRV-infected IECs (2%–12%) in ABX-treated *Ifnlr1*^{-IEC} neonates compared to controls (~1% infected IECs) (Figures 4G and 4H), and the fluorescence intensity of the mRV antigen within infected IECs was not increased in *Ifnlr1*^{-IEC} IECs compared to controls (Figure 4I). Altogether, these data suggest that the homeostatic IFN- λ signaling inhibits mRV infection independent of the bacterial microbiota.

IFN- λ -stimulated genes exhibit distinct patterns of expression and microbiota dependence during development

The presence of a homeostatic IFN- λ response following ABX treatment does not rule out a role for non-bacterial members of the microbiota, including commensal fungi and viruses. Additionally, the hundreds of different ISGs may not follow a uniform pattern of expression during post-natal development. To define the extent of microbiota dependence and ISG heterogeneity in the neonatal homeostatic IFN response, we analyzed a published RNA sequencing (RNA-seq) dataset¹⁵ from the epithelium of germ-free and conventionally housed mice at three stages of development: neonate (1 week), weanling (4 weeks), and adult (12–16 weeks). We compared these six groups of IECs with a gene set from our prior study that defined the homeostatic signature of adult mice.¹⁴ As expected from our prior study, homeostatic ISGs were expressed at lower levels in germ-free weanlings and adults compared to their respective conventionally housed groups (Figure 5A). However, there was no appreciable change in homeostatic ISGs in germ-free neonates compared to their conventionally housed counterparts (Figure 5A). These data are consistent with our qPCR data from ABX-treated mice in the present study (Figures 4C–4E) and indicate that a homeostatic ISG response in neonates is independent of microbiota in its entirety, including commensal fungi and viruses.

To more comprehensively assess heterogeneity among epithelial ISGs, we expanded our analysis of the dataset from Pan et al. to assess the expression of IFN- λ -stimulated genes defined by our prior RNA-seq analysis of IFN- λ -injected neonatal mice.¹³ Hierarchical clustering of all IFN- λ -stimulated genes indicated that neonate IECs from conventional or germ-free housing were indistinguishable, but all neonate groups were clearly distinct from weanling and adult groups (Figure 5B; Table S1A). In contrast to neonates, weanlings and adults were separated into distinct sub-clusters of germ-free and conventional housing (Figure 5B). There was marked heterogeneity in the patterns of ISG expression, and hierarchical clustering divided them into two major clusters (Figures 5B–5D). Cluster 1 ISGs were significantly higher in neonates compared to either weanlings or adults (Figure 5C). In contrast, cluster 2 ISGs were significantly lower in neonates compared to either weanlings or adults (Figure 5D). ISGs in both clusters were not significantly different in germ-free neonates compared to con-

ventional counterparts but were significantly lower in germ-free weanlings or adults compared to conventionally housed counterparts (Figures 5C and 5D). These analyses indicate that the composition of homeostatic ISGs is distinct in neonatal IECs compared to weanlings and adults, with heterogeneity in the directional change in ISG expression (i.e., cluster 1 vs. 2) over the course of development. Regardless of the directional change during development, all homeostatic ISGs in neonatal epithelia are microbiota independent. Thus, homeostatic ISG expression by neonatal IECs is mechanistically distinct from homeostatic ISG expression by adult IECs.

To better understand the differentially regulated ISGs of neonate vs. adult IECs, we compared the features and ontology of ISGs in clusters 1 and 2. We did not find any difference between the clusters in fold change stimulation by IFN- λ treatment (Figure 5E), indicating they were not distinguished by the magnitude of IFN- λ responsiveness. Additionally, Gene Ontology (GO) pathway analysis (Figure 5F; Tables S1B and S1C) revealed highly significant association of both clusters with immune pathways (e.g., innate immune response). However, there were several GO pathways more significantly associated with cluster 1 ISGs (e.g., regulation of the viral life cycle) or cluster 2 ISGs (e.g., response to type II IFN) (Figure 5F). The greater association of cluster 2 ISGs with the type II IFN response pathway suggested that their promoters may have stronger gamma-activated sequence (GAS) motifs, which are activated by STAT1 homodimers downstream of IFN signaling. Comparison of promoter motif scores in promoters of ISGs from each cluster indicated that both clusters had highly significant IFN-stimulated response element (ISRE) motif scores (Figure 5G; Table S1D), consistent with their similar fold change stimulation by IFN- λ treatment (Figure 5E), but only cluster 2 had significant GAS motif scores (Figure 5H; Table S1D). Additional analysis of transcription factor motifs revealed that cluster 2 ISGs had higher motif scores for the repressive transcription factor Prdm1 (also known as Blimp1) (Figure 5I; Table S1D).

Prdm1 plays an essential IEC-intrinsic role in intestinal development, with high expression in neonate IECs and low expression in adult IECs.^{16,17} The higher Prdm1 scores for cluster 2 ISGs are consistent with their lower expression in neonatal IECs (Figures 5B and 5C). To directly test the relationship between Prdm1 expression and ISGs, we re-analyzed published microarray data for intestinal tissue from post-natal day (P)7 neonates with the knockout of Prdm1 in IECs (*Prdm1*^{-IEC})¹⁷ and found that cluster 2 ISGs were significantly decreased in WT vs. *Prdm1*^{-IEC} compared to cluster 1 ISGs (Figure 5J). Together, these data suggested that ISG clusters are developmentally regulated, with one set of antiviral ISGs (cluster 1) highly expressed in neonatal IECs and another set of ISGs with more diverse ontology (cluster 2) that are repressed in neonatal IECs by high expression of Prdm1. Taken together with the preceding data, these analyses suggest a developmentally programmed IFN- λ response that promotes antiviral gene expression (including *Ifit1* and *Isg15*) in the intestinal epithelium of neonates.

Homeostatic ISGs are widely distributed in the neonatal epithelium

Homeostatic ISGs in the SI of adult mice are highly localized within discrete pockets of epithelia, usually within single villus

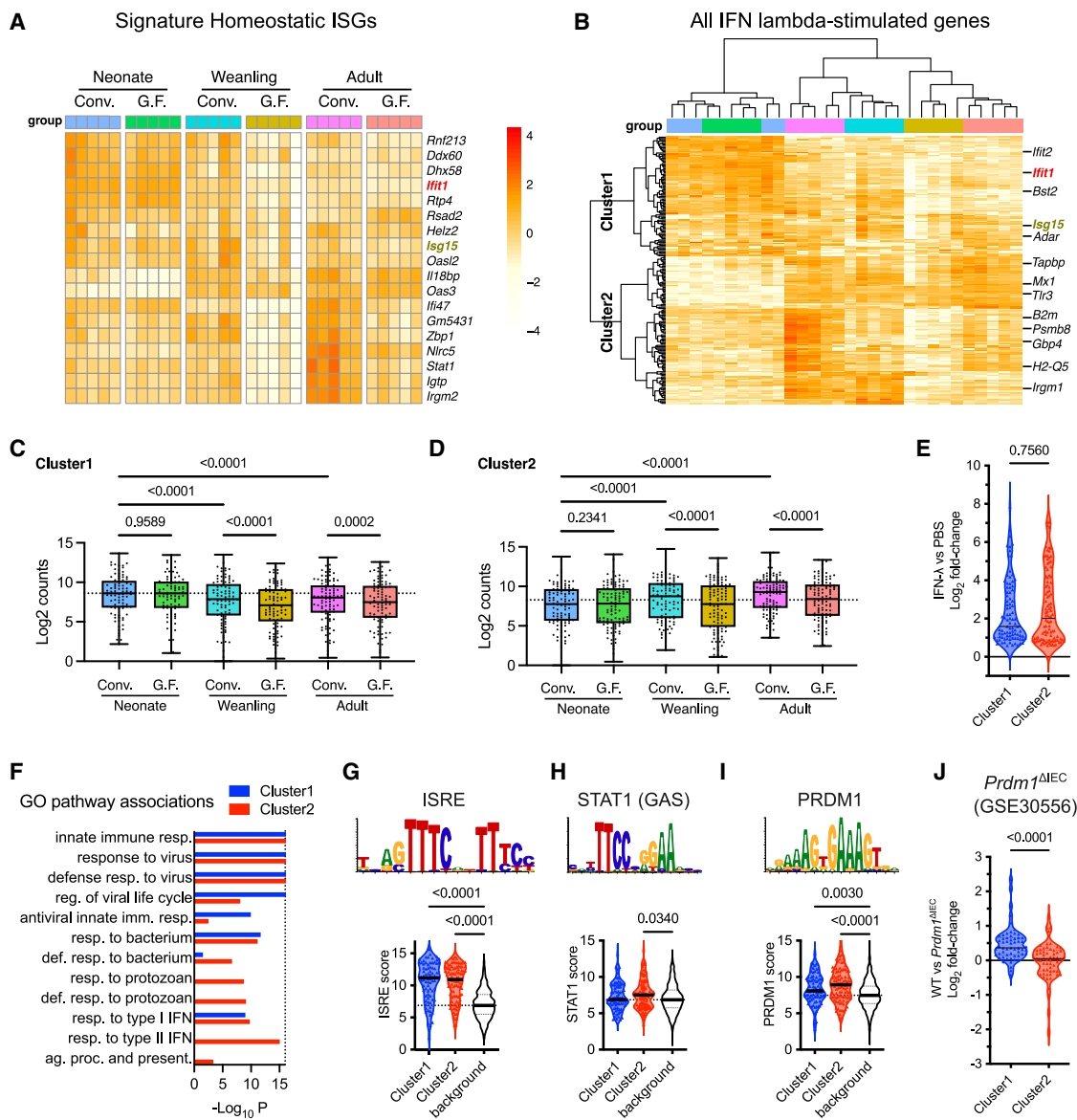


Figure 5. Interferon-lambda-stimulated genes exhibit distinct patterns of expression and microbiota dependence during development

Analysis of ISG expression in IECs from different developmental stages and germ-free housing published previously.¹⁵ Neonate, 1 week; Weanling, 4 weeks; Adult, 12–16 weeks; Conv., conventional housing; G.F., germ-free housing.

(A and B) Heatmaps showing gene expression scaled and centered by row.¹⁴

(A) Expression within the indicated IEC groups of IFN- λ -dependent homeostatic ISGs identified in our prior study of adult mice.¹⁴

(B) Expression within the indicated IEC groups of all IFN- λ -stimulated genes identified in our prior study of IFN- λ -injected neonatal mice.¹³ Clustering was done by Ward's method with squared Euclidian distances. The two major clusters of ISGs are labeled.

(C and D) Comparison of expression levels within each group for ISG cluster 1 (C) and ISG cluster 2 (D) as identified labeled in the heatmap (B). The dashed line indicates the median of the conventionally housed neonate group.

(E) Comparison of ISG cluster 1 and 2 IFN- λ -stimulated fold changes as defined in our prior study of IFN- λ -injected neonatal mice.¹³

(F) Selected Gene Ontology (GO) pathway associations for ISG clusters 1 and 2.

(G–I) Comparison of top scores for the indicated transcription factor motifs in promoters of ISG cluster 1 or 2 or randomly selected gene promoters (background). Sequence logos show promoter motif sequences, with the height of each base reflecting the contribution to the motif score.

(J) Comparison of ISG cluster 1 and 2 log2 fold change expression in WT intestines relative to *Prdm1*^{ΔIEC} intestines from GEO: GSE30556.¹⁷

Statistical significance was determined by one-way repeated-measures ANOVA with the Sidak multiple comparison test (C and D), Kruskal-Wallis test with Dunn's multiple comparison test (G–I), or Mann-Whitney test (E and J). Data in (C) and (D) are represented as boxes at the 25th–75th percentile and whiskers \pm minimum to maximum.

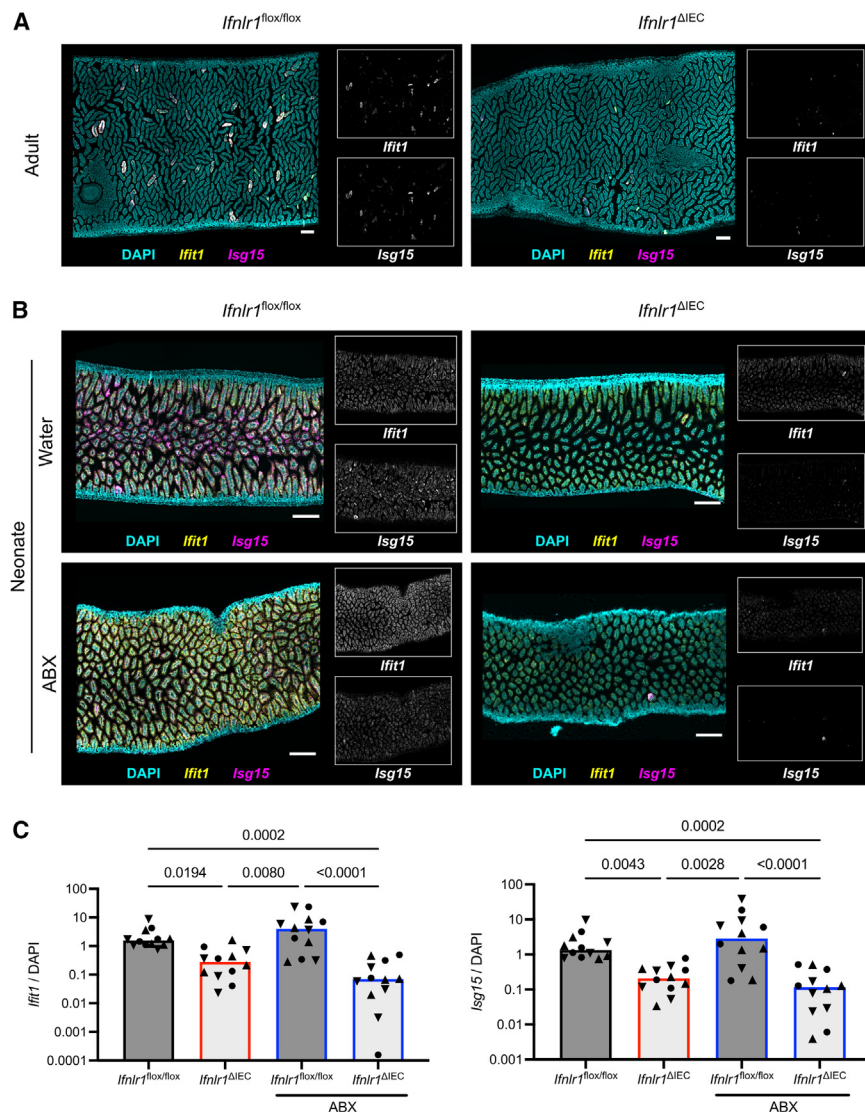


Figure 6. Homeostatic ISGs are widely distributed in the neonatal epithelium

(A and B) Small intestine tissues were stained by *in situ* hybridization for *Ifit1* (yellow) and *Isg15* (magenta), with a DAPI (blue) counterstain.

(A) Representative images of adult *Ifnlr1*^{fl/fl} (left) and *Ifnlr1*^{ΔIEC} (right) small intestine.

(B) Representative images of medial small intestine from neonatal *Ifnlr1*^{fl/fl} (left) and *Ifnlr1*^{ΔIEC} (right) mice provided with conventional water (top) or ABX water (bottom). Scale bars indicate 200 μ m.

(C) Quantitation of *Ifit1* (left) and *Isg15* (right) as a ratio of ISG area to DAPI area. Each data point represents the quantitation of ISGs in proximal small intestine (triangle), medial small intestine (circle), and distal small intestine (downward triangle) from four mice.

Statistical significance was determined by Kruskal-Wallis with Dunn's multiple comparisons test.

mice are widely distributed across the SI, in contrast to the localized pattern of expression in adult mice.

Maturation of the intestinal epithelium regulates homeostatic ISG expression

To better define developmental timing for the shift in spatial distribution of homeostatic ISGs from a pervasive to localized pattern, we visualized ISG expression in intestines of mice at the latter end of the sucking stage (P14) or after weaning (P28). The P14 suckling mice had a mixed phenotype, with less widespread ISG expression and several localized pockets of particularly intense staining (Figure 7A). P28 weanling mice appeared similar to adults, with localized ISG expression

(Figure 7A). These data suggest that the shift of ISG distribution from pervasive to localized occurs gradually in the suckling-to-weanling transition.

Profound changes in the physiology of the small intestinal epithelium occur during the suckling-to-weanling transition, including decreased macromolecule uptake and increased expression of digestive enzymes, such as sucrase isomaltase (*Sis*).¹⁸ These changes are associated with major epigenetic shifts driven in part by *Prdm1* downregulation during maturation.^{15–17} This maturation is driven by an increase in serum corticosteroids, and the administration of exogenous cortisone acetate (CAC) can trigger a premature maturation program in the intestinal epithelium of suckling rodents.^{19,20} To test the effect of premature intestinal maturation on IFN- λ -stimulated homeostatic ISGs in suckling mice, we injected P7 mice with CAC and collected intestinal tissues at P10 for qPCR and imaging (Figures 7B–7E). Maturation indicator genes *Sis* and *Prdm1* were, respectively, increased and decreased in the distal ileum

units.¹⁴ To determine the localization of homeostatic ISGs in neonates, we collected the SIs from 1-week-old neonatal mice or adult controls and stained for ISGs by *in situ* hybridization (Figures 6A–6C). In adult controls, *Ifit1* was infrequently detected in localized pockets (e.g., a single villus) of *Ifnlr1*^{fl/fl} SIs (Figure 6A), confirming our prior findings. Staining for *Isg15* revealed a similar pattern of expression in adult *Ifnlr1*^{fl/fl} SIs, with co-localization to the same regions containing *Ifit1* (Figure 6A). Both *Ifit1* and *Isg15* were nearly undetectable in adult *Ifnlr1*^{ΔIEC} mice, confirming the requirement of IFN- λ signaling on IECs for this homeostatic ISG expression (Figure 6A). In contrast to adults, neonatal *Ifit1* and *Isg15* were detected in a widely distributed pattern across the SIs of *Ifnlr1*^{fl/fl} mice from conventional water or ABX housing conditions (Figures 6B and 6C). Both *Ifit1* and *Isg15* were significantly reduced in the SIs of neonatal *Ifnlr1*^{ΔIEC} mice from conventional water or ABX housing conditions compared to *Ifnlr1*^{fl/fl} intestines (Figures 6B and 6C). Overall, these data indicate that homeostatic ISGs in neonatal

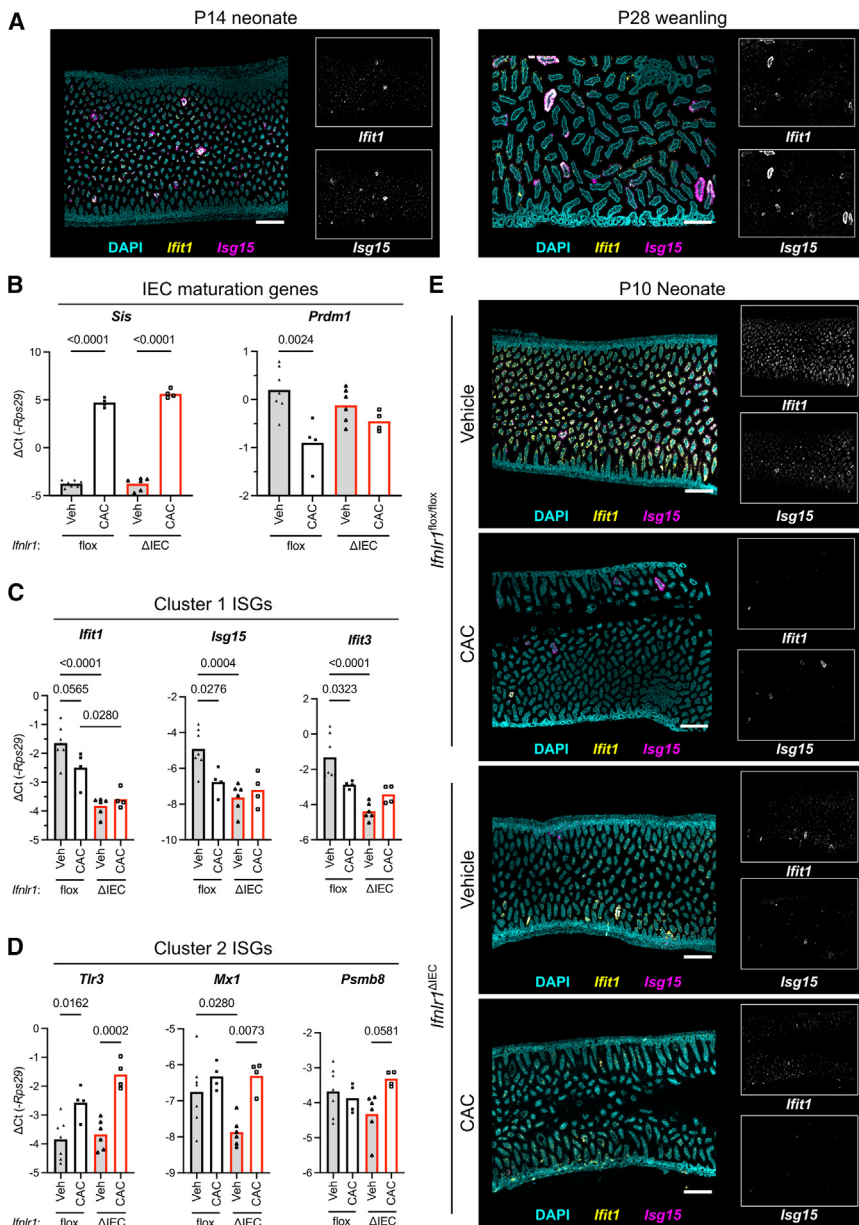


Figure 7. Maturation of the intestinal epithelium regulates homeostatic ISG expression

(A) Small intestine tissues from neonates at P14 (left) or weanlings at P28 (right) were stained by *in situ* hybridization for *Ifit1* (yellow) and *Isg15* (magenta), with a DAPI (blue) counterstain.

(B–E) Littermate *Ifnlr1^{fl/fl}* and *Ifnlr1^{ΔIEC}* neonates were injected with cortisone acetate (CAC) or vehicle (Veh) at P7, and small intestinal tissues were collected at P10.

(B–D) qPCR from distal small intestinal tissue for indicated genes representative of epithelial maturation (B), cluster 1 ISGs (C), or cluster 2 ISGs (D). Statistical significance was determined by one-way ANOVA with the Tukey multiple comparison test.

(E) Medial small intestinal tissues were stained and imaged as in (A).

Each data point in (B)–(D) represents an individual mouse and is cumulative from four litters of mice. Scale bars indicate 200 μ m.

these data suggested that the homeostatic ISG profiles of neonatal intestines are developmentally programmed, with increased and pervasive expression of cluster 1 antiviral ISGs within the neonatal epithelium. This pervasive ISG expression at homeostasis may be part of a pre-emptive antiviral response that protects neonatal mice immediately following viral exposure (Figures 1, 2, and 5).

DISCUSSION

Here, we discover a homeostatic IFN- λ response in the neonatal intestine that is widely distributed across the epithelial surface (Figure 6) and present from birth (Figure 3) but independent of colonization by microbiota (Figures 4, 5, and 6). The neonatal homeostatic IFN- λ response is independent of a maternal source of IFN- λ cytokine but depends on IFN- λ

produced by the neonate (Figure S3). These IEC-intrinsic responses to IFN- λ in the neonatal intestine have a substantial protective role during the first day after exposure to mRV (Figures 1 and 2) that translates to protection from diarrheal disease (Figures 2F and 2G). We conclude that an intrinsic developmental program in the neonatal intestine drives a homeostatic IFN- λ response at birth and is an impactful component of innate antiviral resistance in the newborn intestinal epithelium.

Our study is distinguished from prior work in its focus on homeostatic IFN- λ responses in IECs. This pre-existing antiviral gene expression may underlie an IEC-specific role for IFN- λ within the first day after mRV exposure (Figures 1 and 2). Prior studies have focused on later times P.I. and did not consistently observe a protective role for IFN- λ .^{11,22} Our results are most

tissue following CAC treatment (Figure 7B), confirming the efficacy of treatment. We quantified the expression of cluster 1 ISGs (*Ifit1*, *Isg15*, and *Ifit3*) and found that their expression was reduced by CAC treatment in an IFN- λ -dependent manner (not altered in *Ifnlr1^{ΔIEC}* neonates; Figure 7C). We additionally quantified the expression of cluster 2 ISGs (*Tlr3*, *Mx1*, and *Psmb8*) and found that their expression was increased by CAC treatment in an IFN- λ -independent manner (increased in *Ifnlr1^{ΔIEC}* neonates; Figure 7D). Increased expression of *Tlr3* with CAC treatment was particularly robust and is consistent with a previous report of increased expression with age.²¹ Imaging of cluster 1 ISGs *Ifit1* and *Isg15* corroborated qPCR data, showing decreased expression in IECs following CAC treatment of *Ifnlr1^{fl/fl}*, but not *Ifnlr1^{ΔIEC}*, neonates (Figure 7E). Together,

closely aligned with the prior findings of Pott et al. in showing a protective role for IFN- λ , whereas Lin et al. did not observe a difference in mRV infection in IFN- λ -receptor-deficient mice. One point of distinction between these prior mRV studies is that the WT mice in Pott et al. were not all detectably infected,¹¹ whereas 100% of WT controls in Lin et al. became infected and developed diarrheal disease.²² WT mice in our lab were not all detectably infected at 24 h P.I. (Figures 1 and 2), and only ~70% went on to develop diarrheal disease (Figure 2G). Therefore, we conclude that observation of increased mRV infection in *Ifnlr1*-deficient mice requires experimental models in which WT mice are submaximally infected, and the first cycles of mRV replication are when a role of homeostatic IFN- λ is most relevant.

Our prior studies of homeostatic IFN- λ in adult mice demonstrated stimulation by bacterial microbiota colonization.¹⁴ Additionally, several other studies have indicated a role for microbiota in rotavirus immunity.^{23,24} In this study, we hypothesized that there would be little to no expression of homeostatic ISGs at birth and an increasing expression of ISGs as mice became robustly colonized by bacterial microbiota into adulthood. Instead, we found that homeostatic IFN- λ responses are already present within days of birth (Figures 3B–3J), and this neonatal IFN- λ response does not require colonization by bacterial microbiota (Figures 4C–4E and 5). Additionally, the pattern of expression for neonatal IFN- λ -stimulated genes is widespread as opposed to the highly localized pattern observed in adults (Figure 6). Together, our new data indicate that the neonatal homeostatic IFN- λ response is mechanistically distinct from that of adults.

Our re-analysis of RNA-seq data from IECs of germ-free mice published by Pan et al. indicated that neonatal homeostatic ISGs are expressed in the absence of all commensal microbiota, including bacteria, fungi, and viruses (Figure 5). These data additionally confirmed that neonatal ISG expression in IECs was not unique to mice in our facility. There are hundreds of different ISGs that can be stimulated by IFN- λ , but not all follow a similar pattern of expression between neonate and adult: some ISGs are more highly expressed in neonates than adults (Figure 5C, cluster 1), and others are expressed more highly in adulthood (Figure 5D, cluster 2). Notably, all clusters of ISG are reduced in germ-free adult IECs relative to conventionally housed counterparts but are independent of microbiota in neonates (Figures 5C and 5D). The microbiota independence of homeostatic ISGs in the neonatal epithelium suggests an intrinsic developmental program controlling their expression that is triggered by non-microbial stimuli.

The intestinal epithelium undergoes profound changes during the suckling-to-weanling transition, driven in part by increasing serum corticosteroids and decreasing Prdm1 expression.^{15–19} We find that the pervasive pattern of homeostatic ISG expression in neonates is diminished during the suckling-to-weanling transition (Figure 7A) and is prematurely reduced following cortisone-triggered maturation of the intestinal epithelium (Figure 7E). This reduced expression is specific to cluster 1 ISGs and dependent on IEC expression of the IFN- λ receptor (Figure 7C). This suggests that homeostatic IFN- λ is developmentally programmed in neonatal intestines, but it remains possible that cortisone directly suppresses IFN- λ production independently of the IEC maturation process. Cluster 2 ISGs are increased by

cortisone treatment, in conjunction with reduced expression of Prdm1 and independent of IFN- λ receptor expression on IECs (Figure 7D). These data, together with analysis of *Prdm1*^{ΔIEC} intestines (Figure 5J), suggest that a subset of ISGs are developmentally suppressed in a Prdm1-dependent manner. The evolutionary benefit of differential ISG regulation during development of the intestine is not entirely clear, but we speculate that it may relate to maximizing antiviral protection while minimizing the potential for pathological reactivity to newly acquired microbiota. The presence of antibacterial genes among cluster 2 ISGs supports this hypothesis (Figure 5F).

Non-microbial stimuli for homeostatic ISGs in the newborn intestine could come from maternal sources, such as the constitutive IFN- λ produced by placental trophoblasts²⁵ or oral IFN expressed in breast milk.²⁶ We ruled out these maternal sources of IFN- λ by showing that homeostatic IFN- λ responses are not present in embryonic SIs *in utero* (Figures 3K and 3L), and homeostatic IFN- λ responses are not dependent on the mother's ability to produce IFN- λ (Figure S3). Therefore, the specific postnatal stimuli that trigger homeostatic IFN- λ remain unclear and may reflect a combination of profound changes in enteric biology that occur after birth as the intestine becomes the source of nutrient acquisition. Prior work from us and others indicates that prophylactic administration of exogenous IFN- λ can reduce mRV replication,^{11,13,22} so it is likely that variation in the stimuli that trigger endogenous IFN- λ in neonates will also have a significant impact on their susceptibility to infection. It will be important to identify these specific genetic or environmental variables so we can better understand their role in homeostatic immunity.

In sum, our present study has shown that homeostatic IFN- λ signaling is present in the intestinal epithelium of neonatal mice, independent of the microbiota, mechanistically distinct from the corresponding homeostatic IFN- λ signaling in adult mice, and important for preemptive protection from viral infection. These findings emphasize the importance of IFN- λ in antiviral protection of the gut and indicate that homeostatic expression of IFN- λ is an intrinsic property of the developing neonatal intestine.

Limitations of the study

This study builds on a large body of prior literature showing that IFN- λ provides antiviral protection of the intestinal epithelium. Like many of these prior studies, our conclusions here are limited by the use of mouse models, which may not fully reflect human intestinal biology. Our selection of indicator ISGs for use in qPCR and imaging is a limitation because not all ISGs may not be uniformly regulated, as emphasized by RNA-seq analyses in Figure 5. Similarly, our imaging analyses focused on ISG expression in the SI, but the pattern and extent of ISG expression in the colonic epithelium may differ substantially. Finally, we have thus far been unable to directly detect IFN- λ produced in whole intestinal tissue at homeostasis and will likely need to enrich the source cells to detect its production directly. Instead, we have used ISG expression changes in *Ifnlr1* or *Ifnl2/3* knockouts as an indicator of homeostatic IFN- λ activity. The direct detection of IFN- λ may be possible in the future once we have identified the specific non-microbial stimulus and cell type required for the production of IFN- λ in the neonatal intestine.

RESOURCE AVAILABILITY

Lead contact

Further information and requests for resources and reagents should be directed to and will be fulfilled by the lead contact, Timothy J. Nice (nice@ohsu.edu).

Materials availability

This study did not generate new unique reagents.

Data and code availability

- This paper analyzes existing, publicly available data, accessible at the NCBI Gene Expression Omnibus. Accession numbers are listed in the [key resources table](#).
- Code used to analyze data is available from the [lead contact](#) upon request.
- All other data reported in this paper will be shared by the [lead contact](#) upon request.

ACKNOWLEDGMENTS

Some figure images were created with [BioRender.com](#). The authors would like to thank the following OHSU Core facilities for assistance with this project: the Advanced Light Microscopy Core, the Flow Cytometry Core, and the Histopathology Shared Resource. B.R.R., S.M., K.A.M., B.B., A.P.W., D.A.C., and T.J.N. were supported by National Institutes of Health grant R01-AI130055. B.R.R. was additionally supported by National Institutes of Health grant R25-GM134978. K.A.M. was additionally supported by National Institutes of Health grant T32-GM142619. The funders had no role in the study design, data collection and interpretation, or decision to submit the work for publication.

AUTHOR CONTRIBUTIONS

Conceptualization, T.J.N. and B.R.R.; methodology, B.R.R., D.A.C., and T.J.N.; investigation, B.R.R., S.M., K.A.M., B.B., A.P.W., D.A.C., and T.J.N.; writing – original draft, B.R.R. and T.J.N.; writing – review & editing, B.R.R., S.M., K.A.M., B.B., A.P.W., D.A.C., and T.J.N.; funding acquisition, T.J.N.; supervision, T.J.N. and D.A.C.

DECLARATION OF INTERESTS

The authors declare no competing interests.

STAR★METHODS

Detailed methods are provided in the online version of this paper and include the following:

- [KEY RESOURCES TABLE](#)
- [EXPERIMENTAL MODEL AND STUDY PARTICIPANT DETAILS](#)
 - Mice
- [METHOD DETAILS](#)
 - Antibiotics treatments
 - Rotavirus production and infection
 - Disease scoring
 - Cortisone treatment
 - Epithelial cell isolation
 - Nucleic acid isolation
 - Quantitative PCR
 - Flow cytometry
 - RNAscope
 - Promoter motif and pathway analysis
- [QUANTIFICATION AND STATISTICAL ANALYSIS](#)

SUPPLEMENTAL INFORMATION

Supplemental information can be found online at <https://doi.org/10.1016/j.celrep.2025.115243>.

Received: August 5, 2024

Revised: November 8, 2024

Accepted: January 8, 2025

Published: February 1, 2025

REFERENCES

1. Platts-Mills, J. a, Babji, S., Bodhidatta, L., Gratz, J., Haque, R., Hvat, A., McCormick, B.J., McGrath, M., Olortegui, M.P., Samie, A., et al. (2015). Pathogen-specific burdens of community diarrhoea in developing countries: a multisite birth cohort study (MAL-ED). *Lancet Global Health* 3, e564–e575. [https://doi.org/10.1016/S2214-109X\(15\)00151-5](https://doi.org/10.1016/S2214-109X(15)00151-5).
2. Burns, J.W., Krishnaney, A.A., Vo, P.T., Rouse, R.V., Anderson, L.J., and Greenberg, H.B. (1995). Analyses of Homologous Rotavirus Infection in the Mouse Model. *Virology* 207, 143–153. <https://doi.org/10.1006/viro.1995.1060>.
3. Much, D.H., and Zajac, I. (1972). Purification and Characterization of Epizootic Diarrhea of Infant Mice Virus. *Infect. Immun.* 6, 1019–1024. <https://doi.org/10.1128/iai.6.6.1019-1024.1972>.
4. Wolf, J.L., Cukor, G., Blacklow, N.R., Damrauska, R., and Trier, J.S. (1981). Susceptibility of mice to rotavirus infection: effects of age and administration of corticosteroids. *Infect. Immun.* 33, 565–574. <https://doi.org/10.1128/iai.33.2.565-574.1981>.
5. Schneider, W.M., Chevillotte, M.D., and Rice, C.M. (2014). Interferon-stimulated genes: a complex web of host defenses. *Annu. Rev. Immunol.* 32, 513–545. <https://doi.org/10.1146/annurev-immunol-032713-120231>.
6. Sadler, A.J., and Williams, B.R.G. (2008). Interferon-inducible antiviral effectors. *Nat. Rev. Immunol.* 8, 559–568. <https://doi.org/10.1038/nri2314>.
7. Mordstein, M., Neugebauer, E., Ditt, V., Jessen, B., Rieger, T., Falcone, V., Sorgeloos, F., Ehl, S., Mayer, D., Kochs, G., et al. (2010). Lambda interferon renders epithelial cells of the respiratory and gastrointestinal tracts resistant to viral infections. *J. Virol.* 84, 5670–5677. <https://doi.org/10.1128/JVI.00272-10>.
8. Sommereyns, C., Paul, S., Staeheli, P., and Michiels, T. (2008). IFN-Lambda (IFN-λ) Is Expressed in a Tissue-Dependent Fashion and Primarily Acts on Epithelial Cells In Vivo. *PLoS Pathog.* 4, e1000017. <https://doi.org/10.1371/journal.ppat.1000017>.
9. Nice, T.J., Baldridge, M.T., McCune, B.T., Norman, J.M., Lazear, H.M., Artyomov, M., Diamond, M.S., and Virgin, H.W. (2015). Interferon-lambda cures persistent murine norovirus infection in the absence of adaptive immunity. *Science* 347, 269–273. <https://doi.org/10.1126/science.1258100>.
10. Baldridge, M.T., Lee, S., Brown, J.J., McAllister, N., Urbanek, K., Dermody, T.S., Nice, T.J., and Virgin, H.W. (2017). Expression of Ifnlr1 on intestinal epithelial cells is critical to the antiviral effects of interferon lambda against norovirus and reovirus. *J. Virol.* 91, 2079–2116. <https://doi.org/10.1128/JVI.02079-16>.
11. Pott, J., Mahlaköiv, T., Mordstein, M., Duerr, C.U., Michiels, T., Stockinger, S., Staeheli, P., and Hornef, M.W. (2011). IFN-lambda determines the intestinal epithelial antiviral host defense. *Proc. Natl. Acad. Sci. USA* 108, 7944–7949. <https://doi.org/10.1073/pnas.1100552108>.
12. Mahlaköiv, T., Hernandez, P., Gronke, K., Diefenbach, A., and Staeheli, P. (2015). Leukocyte-Derived IFN-α/β and Epithelial IFN-λ Constitute a Compartmentalized Mucosal Defense System that Restricts Enteric Virus Infections. *PLoS Pathog.* 11, e1004782. <https://doi.org/10.1371/journal.ppat.1004782>.
13. Van Winkle, J.A., Constant, D.A., Li, L., and Nice, T.J. (2020). Selective Interferon Responses of Intestinal Epithelial Cells Minimize Tumor Necrosis Factor Alpha Cytotoxicity. *J. Virol.* 94, 10–1128. <https://doi.org/10.1128/JVI.00603-20>.

14. Van Winkle, J.A., Peterson, S.T., Kennedy, E.A., Wheadon, M.J., Ingle, H., Desai, C., Rodgers, R., Constant, D.A., Wright, A.P., Li, L., et al. (2022). Homeostatic interferon-lambda response to bacterial microbiota stimulates preemptive antiviral defense within discrete pockets of intestinal epithelium. *eLife* 11, e74072. <https://doi.org/10.7554/eLife.74072>.
15. Pan, W.-H., Sommer, F., Falk-Paulsen, M., Ulas, T., Best, L., Fazio, A., Kachroo, P., Luzius, A., Jentzsch, M., Rehman, A., et al. (2018). Exposure to the gut microbiota drives distinct methylome and transcriptome changes in intestinal epithelial cells during postnatal development. *Genome Med.* 10, 27. <https://doi.org/10.1186/s13073-018-0534-5>.
16. Harper, J., Mould, A., Andrews, R.M., Bikoff, E.K., and Robertson, E.J. (2011). The transcriptional repressor Blimp1/Prdm1 regulates postnatal reprogramming of intestinal enterocytes. *Proc. Natl. Acad. Sci. USA* 108, 10585–10590. <https://doi.org/10.1073/pnas.1105852108>.
17. Muncan, V., Heijmans, J., Krasinski, S.D., Büller, N.V., Wildenberg, M.E., Meisner, S., Radonjic, M., Stapleton, K.A., Lamers, W.H., Biemond, I., et al. (2011). Blimp1 regulates the transition of neonatal to adult intestinal epithelium. *Nat. Commun.* 2, 452. <https://doi.org/10.1038/ncomms1463>.
18. Lebenthal, A., and Lebenthal, E. (1999). The Ontogeny of the Small Intestinal Epithelium. *JPEEN - J. Parenter. Enter. Nutr.* 23, S3–S6. <https://doi.org/10.1177/014860719902300502>.
19. Daniels, V.G., Hardy, R.N., Malinowska, K.W., and Nathanielsz, P.W. (1973). The influence of exogenous steroids on macromolecule uptake by the small intestine of the new-born rat. *J. Physiol.* 229, 681–695. <https://doi.org/10.1113/jphysiol.1973.sp010160>.
20. Kennedy, E.A., Aggarwal, S., Dhar, A., Karst, S.M., Wilen, C.B., and Baldrige, M.T. (2023). Age-associated features of norovirus infection analysed in mice. *Nat. Microbiol.* 8, 1095–1107. <https://doi.org/10.1038/s41564-023-01383-1>.
21. Pott, J., Stockinger, S., Torow, N., Smoczek, A., Lindner, C., McInerney, G., Bäckhed, F., Baumann, U., Pabst, O., Bleich, A., and Hornef, M.W. (2012). Age-dependent TLR3 expression of the intestinal epithelium contributes to rotavirus susceptibility. *PLoS Pathog.* 8, e1002670. <https://doi.org/10.1371/journal.ppat.1002670>.
22. Lin, J.D., Feng, N., Sen, A., Balan, M., Tseng, H.C., McElrath, C., Smirnov, S.V., Peng, J., Yasukawa, L.L., Durbin, R.K., et al. (2016). Distinct Roles of Type I and Type III Interferons in Intestinal Immunity to Homologous and Heterologous Rotavirus Infections. *PLoS Pathog.* 12, e1005600. <https://doi.org/10.1371/journal.ppat.1005600>.
23. Uchiyama, R., Chassaing, B., Zhang, B., and Gewirtz, A.T. (2014). Antibiotic treatment suppresses rotavirus infection and enhances specific humoral immunity. *J. Infect. Dis.* 210, 171–182. <https://doi.org/10.1093/infdis/jiu037>.
24. Kandasamy, S., Vlasova, A.N., Fischer, D., Kumar, A., Chattha, K.S., Rauf, A., Shao, L., Langel, S.N., Rajashekara, G., and Saif, L.J. (2016). Differential Effects of *Escherichia coli* Nissle and *Lactobacillus rhamnosus* Strain GG on Human Rotavirus Binding, Infection, and B Cell Immunity. *J. Immunol.* 196, 1780–1789. <https://doi.org/10.4049/jimmunol.1501705>.
25. Bayer, A., Lennemann, N.J., Ouyang, Y., Bramley, J.C., Morosky, S., Marques, E.T.D.A., Cherry, S., Sadovsky, Y., and Coyne, C.B. (2016). Type III Interferons Produced by Human Placental Trophoblasts Confer Protection against Zika Virus Infection. *Cell Host Microbe* 19, 705–712. <https://doi.org/10.1016/j.chom.2016.03.008>.
26. Schafer, T.W., Lieberman, M., Cohen, M., and Came, P.E. (1972). Interferon Administered Orally: Protection of Neonatal Mice from Lethal Virus Challenge. *Science* 176, 1326–1327. <https://doi.org/10.1126/science.176.4041.1326>.
27. Dunn, S.J., Burns, J.W., Cross, T.L., Vo, P.T., Ward, R.L., Bremont, M., and Greenberg, H.B. (1994). Comparison of VP4 and VP7 of Five Murine Rotavirus Strains. *Virology* 203, 250–259. <https://doi.org/10.1006/viro.1994.1482>.
28. Peterson, S.T., Kennedy, E.A., Briggle, P.H., Taylor, G.M., Urbanek, K., Bricker, T.L., Lee, S., Shin, H., Dermody, T.S., Boon, A.C.M., and Baldrige, M.T. (2019). Disruption of type III interferon (IFN) genes Ifnl2 and Ifnl3 recapitulates loss of the type III IFN receptor in the mucosal antiviral response. *J. Virol.* 93, e01073-19. <https://doi.org/10.1128/JVI.01073-19>.
29. Schindelin, J., Arganda-Carreras, I., Frise, E., Kaynig, V., Longair, M., Pietzsch, T., Preibisch, S., Rueden, C., Saalfeld, S., Schmid, B., et al. (2012). Fiji: an open-source platform for biological-image analysis. *Nat. Methods* 9, 676–682. <https://doi.org/10.1038/nmeth.2019>.
30. Kolberg, L., Raudvere, U., Kuzmin, I., Adler, P., Vilo, J., and Peterson, H. (2023). g:Profiler—interoperable web service for functional enrichment analysis and gene identifier mapping (2023 update). *Nucleic Acids Res.* 51, W207–W212. <https://doi.org/10.1093/nar/gkad347>.
31. Heinz, S., Benner, C., Spann, N., Bertolino, E., Lin, Y.C., Laslo, P., Cheng, J.X., Murre, C., Singh, H., and Glass, C.K. (2010). Simple Combinations of Lineage-Determining Transcription Factors Prime cis-Regulatory Elements Required for Macrophage and B Cell Identities. *Mol. Cell* 38, 576–589. <https://doi.org/10.1016/j.molcel.2010.05.004>.
32. Hwang, S.Y., Hertzog, P.J., Holland, K.A., Sumarsono, S.H., Tymms, M.J., Hamilton, J.A., Whitty, G., Bertoncello, I., and Kola, I. (1995). A null mutation in the gene encoding a type I interferon receptor component eliminates antiproliferative and antiviral responses to interferons alpha and beta and alters macrophage responses. *Proc. Natl. Acad. Sci. USA* 92, 11284–11288. <https://doi.org/10.1073/pnas.92.24.11284>.

STAR★METHODS

KEY RESOURCES TABLE

REAGENT or RESOURCE	SOURCE	IDENTIFIER
Antibodies		
Purified anti-mouse CD16/32	BioLegend	clone 93, Cat# 101302, RRID:AB_312801
APC anti-mouse CD326 (Ep-CAM)	BioLegend	clone G8.8, Cat# 118214, RRID:AB_1134102
Brilliant Violet 421™ anti-mouse CD45	BioLegend	clone 30-F11, Cat# 103134, RRID:AB_2562559
Rotavirus NCDV Polyclonal Antibody	Thermo Fisher	RRID:AB_561090, Cat# PA1-7241
Goat anti-Rabbit IgG (H + L) Cross-Adsorbed Secondary Antibody, Alexa Fluor™ 555	Thermo Fisher	RRID:AB_2535849, Cat# A-21428
Bacterial and virus strains		
Murine rotavirus	Dunn et al. ²⁷	Strain EC
Chemicals, peptides, and recombinant proteins		
Vancomycin hydrochloride from Streptomyces orientalis	Sigma	Cat# V2002
Neomycin trisulfate salt hydrate	Sigma	Cat# N1876
Ampicillin sodium salt	Sigma	Cat# A9518
Metronidazole	Sigma	Cat# M1547
TRIzol™ Reagent	Thermo Fisher	Cat# 15596018
ProLong™ Gold Antifade Mountant	Thermo Fisher	Cat# P10144
Cortisone 21-acetate	Thermo Fisher	Cat# 448960050
Critical commercial assays		
Zombie Aqua™ Fixable Viability Kit	BioLegend	Cat# 423102
ZymoBIOMICS DNA Miniprep Kit	Zymo Research	Cat# D4304
Zymo Quick-RNA Viral Kit	Zymo Research	Cat# R1035
Direct-zol RNA Miniprep Kits	Zymo Research	Cat# R2050
TURBO DNA-free™ Kit	Thermo Fisher	Cat# AM1907
ImProm-II™ Reverse Transcriptase Kit	Promega	Cat# A3803
PerfeCTa qPCR FastMix II	Quantabio	Cat# 95119
PowerUp™ SYBR™ Green Master Mix for qPCR	Thermo Fisher	Cat# A25742
RNAscope Multiplex Fluorescent v2 kit	Advanced Cell Diagnostics	Cat# 323100
Deposited data		
Transcriptional response of intestinal epithelial cells to type I and III IFN	NCBI Gene Expression Omnibus	GSE142166
The gut microbiome drives distinct methylome and transcriptome changes in intestinal epithelial cells during postnatal development	NCBI Gene Expression Omnibus	GSE94402
VillinCre-Blimpflox mice postpartum day 7	NCBI Gene Expression Omnibus	GSE30556
Experimental models: Organisms/strains		
Mouse: C57BL6/J	The Jackson Laboratory	RRID:IMSR_JAX:000664
Mouse: <i>Ifnl2/3</i> ^{-/-}	Peterson et al. ²⁸	N/A
Mouse: <i>Ifnlr1</i> ^{-/-}	Baldridge et al. ¹⁰	N/A
Mouse: <i>Ifnlr1</i> ^{flox/flox}	Baldridge et al. ¹⁰	N/A
Mouse: <i>Ifnar1</i> ^{-/-}	The Jackson Laboratory	RRID:MMRRC_032045-JAX
Mouse: <i>Vil1</i> -cre	The Jackson Laboratory	RRID:IMSR_JAX:004586
Oligonucleotides		
<i>Ifit1</i> PrimeTime™ qPCR Probe Assay	IDT	assay# Mm.PT.58.32674307
<i>Isg15</i> PrimeTime™ qPCR Probe Assay	IDT	assay# Mm.PT.58.41476392.g
<i>Ifnlr1</i> PrimeTime™ qPCR Probe Assay	IDT	assay# Mm.PT.58.10781457

(Continued on next page)

Continued

REAGENT or RESOURCE	SOURCE	IDENTIFIER
Rps29 PrimeTime™ qPCR Probe Assay	IDT	assay# Mm.PT.58.41476392.g
RNAscope™ Probe - Mm-Iif1-C2	Advanced Cell Diagnostics	#500071-C2
RNAscope™ Probe- Mm-lsg15-O1	Advanced Cell Diagnostics	#559271
murine rotavirus PrimeTime™ qPCR Probe Assay	IDT	N/A
primer1 - GTTCGTTGTGCCTCATTG primer2 - TCGGAACGTACTTCTGGAC probe - AGGAATGCTTCAGCGCTG		
universal bacteria 16s PrimeTime™ qPCR Probe Assay primer1 - GGACTACCAGG GTATCTAACCTGTT primer2 - TCCTACGGGAGGCAGCAGT probe - CGTATTACCCGGGCTGCTGGCAC	IDT	N/A
<i>Sis</i> qPCR Primers primer1 – TGCTTGCT GTGGAAGAAGTAA primer2 – CAGCCACGCTTCACTTACATTT	IDT	N/A
<i>Prdm1</i> qPCR Primers primer1 – AGTTCCAAGAAATGCCAAC primer2 – TTTCCTCCTTAAAGCCATCAA	IDT	N/A
<i>Ifit3</i> qPCR Primers primer1 – CTTCAGCTGTGGAAGGATCG primer2 – CACACCCAGCTTTCCCA	IDT	N/A
<i>Tlr3</i> qPCR Primers primer1 – AAAATCCTTGCCTGCGAAGT primer2 – TGTTCAAGAGGAGGGCGAATAA	IDT	N/A
<i>Mx1</i> qPCR Primers primer1 – GACCATA GGGGTCTTGACCAA primer2 – AGACTTGCTCTTCTGAAAAGCC	IDT	N/A
<i>Psmb8</i> qPCR Primers primer1 – CCATTCC GAAGATAATACAACCTG primer2 – TGCAGGGAGTTACATTAGCTC	IDT	N/A
Software and algorithms		
FlowJo, version 10	Becton Dickinson	RRID:SCR_008520
ZEISS ZEN Microscopy Software, version 3.1	Zeiss	RRID:SCR_013672
ImageJ, version 2.14	Schindelin et al. ²⁹	RRID:SCR_002285
Prism	GraphPad	RRID:SCR_002798
g:Profiler	Kolberg et al. ³⁰	RRID:SCR_006809
HOMER	Heinz et al. ³¹	RRID:SCR_010881
GEO2R	National Institutes of Health	RRID:SCR_016569
JASPAR		RRID:SCR_003030

EXPERIMENTAL MODEL AND STUDY PARTICIPANT DETAILS

Mice

Mouse strains used in this study were bred on the C57BL/6 background and all experiments used littermate-matched experimental and control mice. All mice were bred and maintained in specific pathogen-free facilities at Oregon Health & Science University (OHSU). Animal protocols were approved by the Institutional Animal Care and Use Committee at OHSU (IP00000228) in accordance with standards provided in the Animal Welfare Act. Specific targeted alleles used in this study are *Ifnlrl1^{-/-}* and *Ifnlrl1^{fl/fl}* (generated from *Ifnlrl1^{tm1a(EUCOMM)Wtsi}* as published¹⁰), *Ifnar1^{-/-}* (*Ifnar1^{tm1Agt}*), *Ifnl2/3^{-/-}* (*Ifnl3^{em1Mtba}*), and *Vil1-cre* (*Tg(Vil1-cre)997Gum*). We generated littermate offspring with variable IFN receptor deficiency (*Ifnlrl1^{-/+}/Ifnar1^{-/-}*, *Ifnlrl1^{-/-}/Ifnar1^{-/-}*, *Ifnlrl1^{-/-}/Ifnar1^{-/-}*, *Ifnlrl1^{-/-}/Ifnar1^{-/-}*) by setting up breeding pairs of *Ifnlrl1^{-/-}*/*Ifnar1^{-/-}* and *Ifnlrl1^{-/-}*/*Ifnar1^{-/+}* parents. Use of doubly heterozygous mice as littermate controls is justified because a single copy of IFN receptor has been shown to be sufficient for antiviral protection.³² Mice were used at ages and developmental stages indicated in the figure legends and text. Embryos for data in Figures 3K and 3L were dissected from visibly pregnant dams and developmental stage was estimated based on overall size and morphology of head

and digits. Both sexes were included in all experiments with equal distribution between experimental and control groups whenever possible.

METHOD DETAILS

Antibiotics treatments

Mice were administered an *ad libitum* antibiotics cocktail (ABX): 0.5 g/L vancomycin, 1 g/L neomycin, 1 g/L ampicillin, and 1 g/L metronidazole in deionized H₂O. Mice breeders were on ABX for a minimum of 2 weeks prior to harvest of litter.

Rotavirus production and infection

Mouse rotavirus (EC strain) stocks were generated from gastrointestinal tracts of neonatal mice collected 4 days after inoculation, upon appearance of diarrhea. Intestines were frozen, thawed, suspended in PBS, and homogenized in a bead beater using 1.0 mm zirconia-silica beads (BioSpec Products). These homogenates were clarified of debris, aliquoted, and stored at -70°C until use for infections. The 50% shedding dose (SD50) was determined by inoculation of 10-fold serial dilutions in adult C57BL/6J mice. For experimental infections in this study, neonatal mice were fed twice by pipet with 5 µL volumes of mRV in PBS, resulting in a total inoculum of 500 SD50 in a 10 µL volume. Intestines were isolated 24hr after inoculation and epithelial fractions were isolated for quantitation of viral genomes by qPCR and viral antigen by flow cytometry.

Disease scoring

Diarrhea was monitored daily by applying slight pressure to the abdomen of neonatal mice to induce defecation. Indications of diarrhea were as follows: yellow and non-viscous liquid/liquid fecal content or yellow colored fecal residue near the rectum. If none of the previous indicators were observed the mice were considered as "no diarrhea". The scoring method was performed on a "diarrhea" or "no diarrhea" binary scale.

Cortisone treatment

Cortisone acetate was prepared for injection by preparing a fine suspension in PBS with 2% Tween-80 at 25 mg/mL, aliquoting, and freezing at -20°C. Aliquots were thawed and sonicated at 37°C for 1 min prior to use, and vortexed between injections to maintain suspension. P7 neonates were injected subcutaneously with 0.5 mg/g, or with equivalent volume of vehicle control, and intestinal tissues were collected on P10.

Epithelial cell isolation

Epithelial fractions were obtained from intestines as previously published.¹⁴ Briefly, mouse small intestine was opened longitudinally and rinsed of contents in PBS. Intestines were placed in strip buffer consisting of PBS with 10% fetal calf serum, 15mM HEPES, 5mM EDTA, and 5mM dithiothreitol, followed by moderate agitation at 37°C for 20 min. Liberated cells were passed through cell strainers and used for qPCR or flow cytometry analyses as described.

Nucleic acid isolation

DNA was isolated from the colon contents using the ZymoBIOMICS DNA Miniprep Kit (Zymo Research).

RNA was isolated from harvested tissue or IECs using TRIzol (Thermo Fisher) or Direct-zol (Zymo Research). For samples with ethanol contamination (assessed by high 230/260 ratio), RNA was additionally purified using the Zymo Quick-RNA Viral Kit (Zymo Research). DNA contamination was removed using the Turbo DNA-free kit (Thermo Fisher).

Quantitative PCR

Complementary DNA was synthesized from purified RNA using the ImProm-II reverse transcriptase system (Promega). Quantitative PCR for *Ifit1*, *Isg15*, *Rps29*, murine rotavirus, and 16s rDNA was performed using PerfeCTa qPCR FastMix II (Quantabio). Quantitative PCR for *Sis*, *Prdm1*, *Ifit3*, *Tlr3*, *Mx1*, and *Psmb8* was performed using PowerUp SYBR Green Master Mix (Thermo Fisher).

Flow cytometry

Cells collected from epithelial fractions were stained with Zombie Aqua viability dye (BioLegend) and Fc receptor-blocking antibody (BioLegend) in PBS, followed by staining with anti-EpCAM (BioLegend), and anti-CD45 (BioLegend). Cells were fixed in 4% paraformaldehyde for 10 min at room temperature, followed by washing in PBS and permeabilization in PBS with 0.1% Triton X-100 with 3% fetal calf serum. Murine rotavirus was detected by staining fixed/permeabilized cells with rotavirus polyclonal antisera (Thermo Fisher) followed by goat anti-rabbit secondary conjugated to Alexa 555 (Thermo Fisher). Data was analyzed using FlowJo software.

RNAscope

Intestinal tissues were fixed in 10% neutral-buffered formalin for 18–24 h, followed by rinsing and storage in 70% ethanol. Intestinal segments were cut and placed in a block of 2% agar, with arrangement of parallel segments from proximal to distal small intestine. Tissues were paraffin-embedded and sections cut at 5 µm thickness. RNA *in situ* hybridization was performed using the RNAscope

Multiplex Fluorescent v2 kit (Advanced Cell Diagnostics) per protocol guidelines. Staining with anti-sense probes for detection of *Ifit1* and *Isg15* was performed using ACDBio protocols and reagents. Slides were stained with DAPI and mounted with ProLong Gold antifade reagent (Thermo Fisher) and imaged using a Zeiss ApoTome2 on an Axio Imager, with a Zeiss AxioCam 506 (Zeiss). Intestinal segments were collected separately for each mouse as a stitched image and all images were processed using Zeiss Zen 3.1 software. Signal from unstained control slides was used to set background values for determination of ISG area on experimental images. ISG probe area was normalized to DAPI area to control for different total tissue sizes among the segments that were analyzed. Figures were prepared using ImageJ.

Promoter motif and pathway analysis

Position weighted motif matrix files were obtained from the JASPAR database for ISRE (MA0517.1), STAT1/GAS (MA0137.2), and PRDM1 (MA0508.1) elements. The findMotifs.pl function from the Hypergeometric Optimization of Motif EnRichment (HOMER) software package was used to obtain scores and locations of motifs in ISG promoters from 2000 basepairs upstream to 500 basepairs downstream of the annotated transcription start site. The highest motif scores for each gene were used to generate the graphs in Figures 5G–5I and are listed in Table S1D.

Gene ontology (GO) pathway enrichment and TRANSFAC motif enrichment for ISG lists were analyzed using g:Profiler and all significant results are listed in Tables S1B and S1C.

Published microarray data (GSE30556) were analyzed using default settings within the GEO2R web tool (<https://www.ncbi.nlm.nih.gov/geo/geo2r/>). Log2 fold-change values within the resulting table of differential gene expression were used to generate the graph in Figure 5J.

QUANTIFICATION AND STATISTICAL ANALYSIS

Sample size estimation was performed based on historical data. Data were analyzed with Prism software (GraphPad). Statistical tests used, value and definition of n, definition of center, dispersion and precision measures can be found in the figure legends.